

Irrelevance of disorder in the superconductor to insulator transition of granular aluminum

Aviv Glezer Moshe,^{1,2,*} Gal Tuvia,¹ Shilo Avraham,^{1,2} Eli Farber,² and Guy Deutscher¹

¹*Raymond and Beverly Sackler School of Physics and Astronomy, Tel Aviv University, Tel Aviv, Israel*

²*Department of Physics and Department of Electrical and Electronic Engineering, Ariel University, P.O.B. 3, Ariel 40700*

(Dated: January 14, 2021)

We find excellent agreement between tunneling and optical conductivity gap values in superconducting granular aluminum films, up to the Metal to Insulator transition. This behavior, in strong contrast with that recently reported in atomically disordered samples for which the optical gap becomes smaller than the tunneling gap, rules out disorder as being at the origin of the transition. Rather, it confirms that it is of the Mott type. The large increase seen in the strong coupling ratio is interpreted as a sign of a BCS to BEC cross over, consistent with a Mott transition.

I. INTRODUCTION

A superconductor (SC) can be turned into insulator by increasing disorder on the atomic scale, i.e. by adding impurities such as Nitrogen vacancies in NbN_x [1–5] or Oxygen vacancies in InO_x [5, 6]. It was found that the superconducting gap as indicated by the absorption threshold for photons, namely Ω , is decreasing faster than the one measured by tunneling, namely Δ , as disorder increases. Possible explanations for this deviation are the emergence of a Higgs mode [5] or a re-normalization of the gap predicted by Larkin and Ovchinnikov (LO) [7] which shows good agreement with experiment [4]. Upon increasing disorder further, the superconductor undergoes a metal-to-insulator (M/I) Anderson transition when the product $k_F l$ approaches unity, where k_F is the Fermi wave vector and l is the mean free path.

We show here that this behavior is not a general property of superconductors approaching a M/I transition. In granular aluminum (grAl) films, consisting of nano-scale metallic grains weakly coupled together, the energy scales Ω and Δ remain identical up to the M/I transition. According to the theory of LO this implies that disorder plays only a minor role in the metal to insulator transition of grAl, contrary to the case of NbN_x and InO_x . We ascribe this different behavior to a Mott transition [8–10], driven by the electrostatic charging energy of the small grain. An increase of the strong coupling factor, expected near a Mott transition, is more clearly observed for 2 nm than for 3 nm grain size samples. This difference is discussed in terms of the larger energy level splitting and electrostatic charging energy in the smaller grain samples.

II. METHODS

The grAl films were prepared by thermally evaporating clean Al pallets under controlled O_2 pressure onto liquid nitrogen cooled substrate or onto room temperature warm substrate, for more details see [9]. The role that the substrate temperature plays is crucial, since it determines the grain size, its distribution and the maximum T_c . For substrates held at room

temperature the maximum T_c is about 2.2 K [11–13] and the grain size is about 3 ± 1 nm [14] whereas for substrates held at liquid nitrogen temperature the maximum T_c is about 3.2 K and the grain size is about 2 ± 0.5 nm [11, 15].

In order to obtain samples with varying normal state resistivity along the phase diagram we varied the O_2 pressure while keeping the deposition rate around 5 ± 1 Å/s. In order to obtain high quality, homogeneous samples, we made sure that the pressure and deposition rate were stable during deposition.

For the tunneling experiments we first evaporate 50 nm of grAl film onto liquid nitrogen cooled Al_2O_3 substrate, patterned to a rectangle with dimensions of 0.5×4 mm, by using a hard mask. After evaporation, we expose the film to atmosphere for a few hours, resulting in a native thin oxide barrier. We then use a second mask to evaporate two 50 nm thick, 0.5 mm wide aluminum strips, perpendicular to the grAl film, resulting in a grAl-oxide-Al tunneling junctions. This geometry allows us to measure as well as tunneling the resistivity of the film vs temperature and therefore determine T_c and the normal state resistivity $\rho_{4.2\text{K}}$ for each sample.

For each junction we took current-voltage (I vs V) and differential conductance-voltage (dI/dV vs V) characteristics using Keithley 6221 current source and Keithley 2182A nanovoltmeter, operated in differential conductance mode. The same set of equipment, operated in delta mode, was used for the resistivity measurements. Measurements were taken in three different systems: a commercial ^3He probe by Quantum Design PPMS with a base temperature of 0.4 K, commercial Oxford Instruments Triton 400 dilution refrigerator with a base temperature of ~ 20 mK and a liquid ^4He bath cryostat with a base temperature of about 1.5 K. A small magnetic field of ~ 0.1 T was applied below ~ 1.5 K in order to suppress the top Al electrode superconductivity.

Each dI/dV spectrum was fitted to a Dynes [16] form, which takes into account the broadening Γ of the coherence peaks due to the recombination time of the quasi-particles. This approach allows us to extract the superconducting gap $\Delta(T \rightarrow 0) = \Delta_0$ and the broadening parameter Γ . For more details on the data analysis, see supplemental material.

Additional samples were prepared on $10 \times 10 \times 2$ mm³ MgO or $10 \times 10 \times 1$ mm³ $(\text{LaAlO}_3)_{0.3}(\text{SrAl}_{0.5}\text{Ta}_{0.5}\text{O}_3)_{0.7}$ (LSAT) substrates, held at room temperature, for THz optical spectroscopy. All samples are 100 nm thick, except the lowest

* avivmoshe@mail.tau.ac.il

resistivity one, which is 40 nm thick. Measurements were done by utilizing a quasi-optical Mach-Zehnder interferometer with backward-wave oscillators (BWO) in a frequency range of 3-17 cm^{-1} (or about 0.1-0.5 THz). Commercial optical ^4He cryostat with a home built sample holder, provides us dynamic temperature range down to 1.5 K. The complex transmission was measured for all samples at 4.2 K and at various temperatures close to and below T_c down to 1.5 K. We then obtain the optical conductivity $\hat{\sigma}(\omega) = \sigma_1(\omega) + i\sigma_2(\omega)$ from the measured complex transmission function. We take $\sigma_1(\omega)$ at 4.2 K as the normal-state conductivity and then fit the resulted $\hat{\sigma}(\omega, T)/\sigma_n$ to Mattis-Bardeen (MB) theory [17], as appropriate for a dirty limit superconductor [9, 18]. The only fitting parameter is $\Omega(T)$ which we fit to the BCS gap equation [19] in order to extract $\Omega(T \rightarrow 0) = \Omega_0$. For more details on the data analysis, see supplemental material.

III. RESULTS

The resistivity curves for selected 2 nm grain samples are shown in Fig. 1, showing the SC transition. We take T_c as the value where the resistivity falls to one percent of its normal state value. Representative differential conductance data for selected samples can be found in the supplemental material. Above the gap, for high resistivity samples, $dI/dV \propto \sqrt{V}$, similarly to Dynes *et al.* [20] observation on grAl samples, deposited on substrates held at room temperature.

The obtained values of Δ_0 and Ω_0 for all 2 nm grain size studied samples are shown in Fig. 2 (Top panel). It can be clearly seen that the optical conductivity and tunneling gaps, remarkably, are in excellent agreement. This point is further illustrated in Fig. 3, where Δ as indicated by the coherence peak position for the tunneling data and Ω by the minimum in $\sigma_{1,s}$ for the optical data are seen to coincide. This is our central result.

In Fig. 4 (Top panel), the trend of increasing coupling ratio previously reported for the optical gap [9, 18] can be clearly seen here for the two sets of data, going up to about 6. This strong increase is a characteristic feature of a BCS-BEC crossover region [21, 22] and strengthens our previous suggestion that such a cross-over occurs near a Mott transition in grAl samples [9].

We can gain more insight on the role of the size of the grain by making a similar comparison between optical and tunneling data for samples with a grain size of 3 nm. A recent study of the gap as measured from the optical response of samples shaped into resonators (deposited at room temperature [13]) shows similar gap values but lower critical temperature values than Dynes *et al.* [12, 20] and this work. We have compared Ω_0 as measured from the optical conductivity data (see supplemental) to the tunneling Δ_0 as measured by Dynes *et al.* [12], see bottom panel of Fig. 2 (for a detailed analysis see supplemental material). As for the case of 2 nm grain size samples, there is a good agreement between the tunneling and optical conductivity gaps. As well, the variation of T_c is in line with the tunneling data. However we see that the coupling ratio (Fig. 4, bottom panel) does not change as rapidly

in comparison to the 2 nm grain size samples. We will go back to this important point later on, and argue that it is a direct consequence of the different grain size and its distribution.

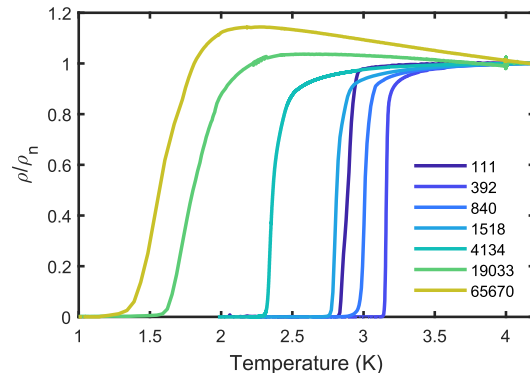


Figure 1. Normalized resistivity curves for selected samples along the phase diagram. The legend corresponds to the normal state resistivity value ρ_n , expressed in $\mu\Omega \text{ cm}$. Note how the transition remains relatively sharp, even for very high resistivity values, for which superconductivity is destroyed in atomically disordered samples such as NbN_x [1–3].

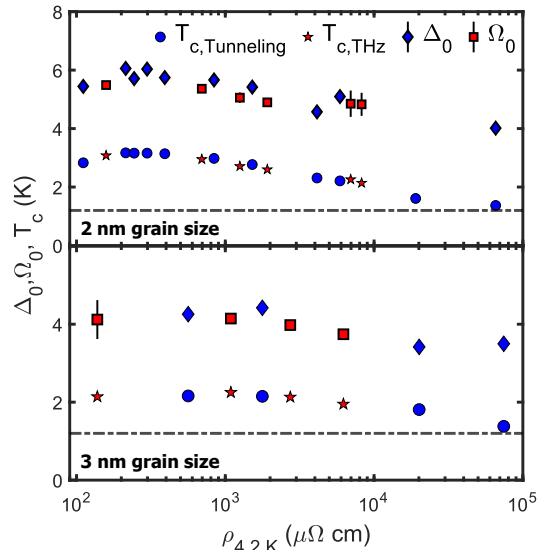


Figure 2. T_c , Δ_0 and Ω_0 vs $\rho_n = \rho_{4.2\text{K}}$. Top: 2 nm grain size samples. Ω_0 is from our previous THz spectroscopy data [9] and Δ_0 is from the tunneling data (this work). Note that for the sample with a resistivity value close to 20,000 $\mu\Omega \text{ cm}$, we only measured T_c due to poor junction quality. Bottom: 3 nm grain size samples. Ω_0 is from THz spectroscopy data (this work) and Δ_0 is from previous tunneling data (Dynes *et al.* [12]). The semi-dashed line marks the T_c of pure Al, 1.2 K. The error bars on Ω_0 (smaller than the symbol size) in the MB fit of $\sigma_1(\omega)$. The error bars on Δ_0 (smaller than the symbol size) reflect the uncertainty in the Dynes fit of the differential conductance.

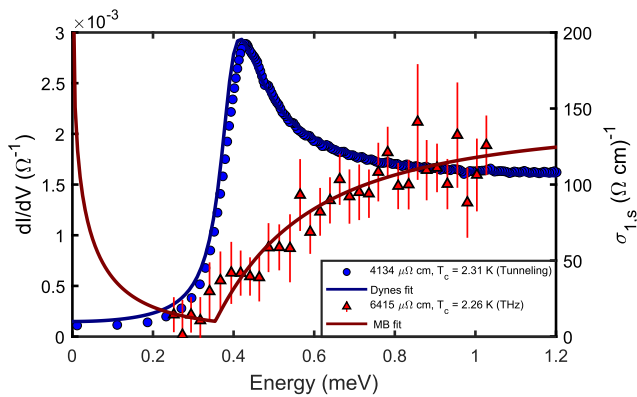


Figure 3. Illustration of the agreement of Δ and Ω in samples (with grain size of 2 nm) with relatively close values of ρ and T_c . The left axis corresponds to the differential conductance dI/dV , taken at 24 mK, along a fit to a Dynes form. The right axis corresponds to the real part of the optical conductivity $\sigma_{1,s}$, taken at 1.5 K, along a fit to MB theory. Note that for the THz data the horizontal axis has been divided by a factor of two to take into account that the absorption threshold corresponds to 2Ω . The error bars on $\sigma_{1,s}$ reflect the experimental accuracy in the optical transmission mainly due to standing waves in the optical cryostat.

A closer look at the tunneling data near T_c reveals that for high resistivity samples the gap is not being fully closed, as it should in a conventional SC. This is well demonstrated in Fig. 5. We note that an anomalously weak temperature dependence of the gap has been predicted to occur in the BCS-BEC cross-over region, as well as an increased strong coupling factor [21, 22]. Therefore the increase in the coupling ratio shown in Fig. 4 along with the anomalous temperature dependence of the gap highly suggests that a BCS-BEC crossover is responsible for our observations.

IV. DISCUSSION

In atomically disordered SC, where the insulating state is of the Anderson type, electrons are being localized by disorder. As disorder increases, the tunneling and optical conductivity gaps are being progressively separated, as was observed in NbN_x [1–5] and InO_x [5, 6]. The separation can be described quite well by the theory of LO [7] which predicts that $\Omega = (1 - \eta^{2/3})^{3/2}\Delta$, where η is a depairing parameter that increases with disorder. This theory shows good agreement with experiment [4].

This is in strike contrast to what we observe, namely there is a good agreement between the tunneling and optical conductivity gaps up to very high resistivity values, much higher than observed in NbN . Hence the disorder parameter introduced by LO plays little role, if any, in the M/I transition of grAl.

Rather we ascribe it to the vicinity of a Mott transition [9], where the effective bandwidth goes to zero. A BCS-BEC

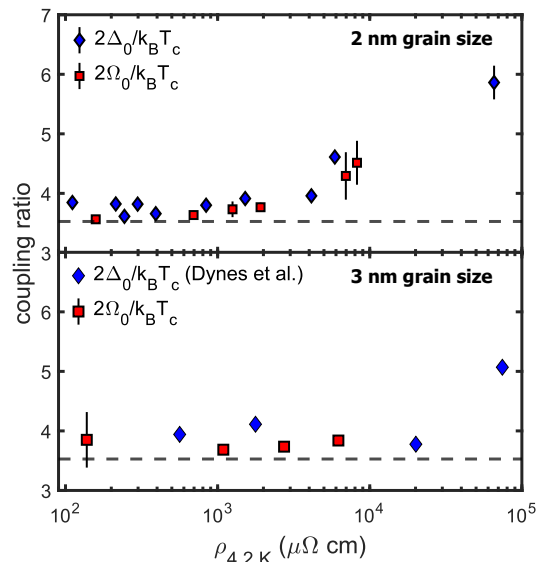


Figure 4. Coupling ratio vs $\rho_n = \rho_{4.2\text{K}}$. Top: 2 nm grain size samples. The values of $2\Omega_0/k_B T_c$ and $2\Delta_0/k_B T_c$ have been obtained from our previous THz spectroscopy data [9] and from this work tunneling data. Bottom: 3 nm grain size samples. $2\Omega_0/k_B T_c$ has been obtained from this work THz spectroscopy data and $2\Delta_0/k_B T_c$ is taken from a previous tunneling work by Dynes et al. [12]. Strikingly, while for the 2 nm grain size samples there is a clear increase of the coupling ratio with the resistivity, already around 2,000 $\mu\Omega\text{cm}$, the increase in the 3 nm grain size samples occurs only above 20,000 $\mu\Omega\text{cm}$. The dashed line marks the BCS weak coupling ratio, 3.53. The error bars reflect the uncertainty in Ω_0 and Δ_0 .

cross-over is expected when it becomes of the order of the gap. The strong increase of the coupling ratio, up to almost two times the BCS weak coupling ratio of 3.53, as well as the weak temperature dependence of the gap, supports this scenario [21, 22]. Recent calculations of a model that takes into account both Mott behavior and SC shows as well that the coupling ratio exceeds that of the BCS weak coupling value [23]. Another piece of evidence which supports this picture is the fact that the coherence length ξ decreases with resistivity down until it saturates to a value of about 6-7 nm (as obtained from upper critical field measurements [24]). This saturation of the coherence length is a characteristic of the BCS-BEC crossover regime [25].

We wish now to discuss more in depth the role of the grain size. It is important as it determines both the charging energy [26, 27] $E_c \propto 1/d$ and the level spacing [27, 28] $\delta \propto 1/d^3$ of the metallic grains. As the grain size is being reduced, the Mott transition and the related BCS-BEC crossover are favored against an Anderson transition.

This is clearly seen in Fig. 2 and 4 where the increase in $2\Delta/k_B T_c$ for 2 nm grain size is highly pronounced, in sharp contrast to the 3 nm grain size data. We can explain this difference by noticing that due to its smaller level spacing a 3 nm grain size is more sensitive to disorder. Most importantly, since the gap value is also smaller for the larger grain size, one needs to be closer to the Mott transition in order to have a reduced Fermi energy which is close to the gap value. Therefore

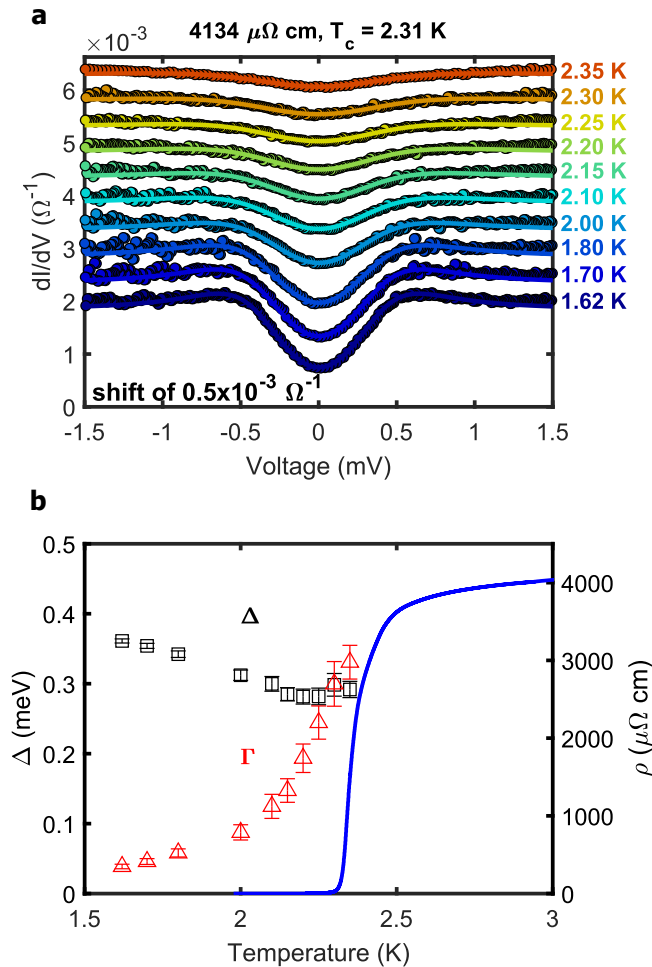


Figure 5. High resistivity data near and below the critical temperature. **(a)** Differential conductance vs voltage, taken close to the critical temperature, along a fit to a Dynes form. The data is shifted for clarity. **(b)** Δ and Γ (left axis in units of meV) vs temperature, as obtained from the fits, along the resistivity ρ (right axis). Note that Δ remains finite near T_c , as predicted in a BCS-BEC crossover scenario near unitarity [21, 22]. The data was taken using a ^4He bath cryostat, prior to the dilution refrigerator measurements (shown in Fig. 3). Note that since the sample sheet resistance was comparable to the junction resistance, we could not take reliable data above T_c . The error bars on Δ and Γ reflect the uncertainty in the Dynes fit of the differential conductance.

the combined effect of the smaller gap value, smaller level spacing and smaller charging energy is that the approach to a BCS-BEC crossover is less likely to occur in larger grain samples.

The importance of the grain size also comes into play when we compare our tunneling results to recent scanning tunneling microscope (STM) results, which have revealed the presence of in-gap states in grAl films having a resistivity of 2,000 micro-ohm cm [29], while we do not see any sign of such states in a higher resistivity film, see Fig. 3. We believe that the reason for this difference is the smaller grain size of our sample, 2 nm as compared to 5 to 10 nm. We note that the in-gap states seem to be more clearly seen in the larger grains.

Regarding further possible applications, in particular ones that involve GHz and sub THz frequencies, grAl should be favored over disordered superconductors, as already proven in several applications of quantum circuits [30–37] using 3 nm grain size films. We have provided here further experimental evidence that grAl with smaller grain size should yield even higher performance devices because of a reduced presence of in-gap states.

In conclusion, we have measured the evolution of the SC gap Δ by tunneling and THz spectroscopy, and have found them to be in good agreement up to the vicinity of the M/I transition. We have shown that the coupling ratio $2\Delta/k_B T_c$ is increasing up to ~ 6 for 2 nm grain size samples, as expected by a BCS-BEC crossover induced by the vicinity to a Mott transition. In these small grain films we have found no evidence for the presence of in-gap states up to normal state resistivity values of several 1,000 $\mu\Omega$ cm.

ACKNOWLEDGEMENTS

Helpful discussions with Ioan Pop and Giancarlo Strinati are gratefully acknowledged. We thank Yoram Dagan for granting us access to his dilution refrigerator.

- [1] M. Chand, G. Saraswat, A. Kamlapure, M. Mondal, S. Kumar, J. Jesudasan, V. Bagwe, L. Benfatto, V. Tripathi, and P. Raychaudhuri, *Phys. Rev. B* **85**, 014508 (2012).
- [2] M. Mondal, M. Chand, A. Kamlapure, J. Jesudasan, V. C. Bagwe, S. Kumar, G. Saraswat, V. Tripathi, and P. Raychaudhuri, *Journal of Superconductivity and Novel Magnetism* **24**, 341 (2011).
- [3] M. Mondal, A. Kamlapure, M. Chand, G. Saraswat, S. Kumar, J. Jesudasan, L. Benfatto, V. Tripathi, and P. Raychaudhuri,

Phys. Rev. Lett. **106**, 047001 (2011).

- [4] B. Cheng, L. Wu, N. J. Laurita, H. Singh, M. Chand, P. Raychaudhuri, and N. P. Armitage, *Phys. Rev. B* **93**, 180511 (2016).
- [5] D. Sherman, U. S. Pracht, B. Gorshunov, S. Poran, J. Jesudasan, M. Chand, P. Raychaudhuri, M. Swanson, N. Trivedi, A. Auerbach, M. Scheffler, A. Frydman, and M. Dressel, *Nature Physics* **11**, 188 (2015).

- [6] D. Sherman, B. Gorshunov, S. Poran, N. Trivedi, E. Farber, M. Dressel, and A. Frydman, *PRB* **89**, 035149 (2014).
- [7] A. Larkin and Y. N. Ovchinnikov, *Sov. Phys. JETP* **34**, 1144 (1972).
- [8] N. Bachar, S. Lerer, A. Levy, S. Hacoheh-Gourgy, B. Almog, H. Saadaoui, Z. Salman, E. Morenzoni, and G. Deutscher, *Physical Review B* **91**, 041123 (2015).
- [9] A. G. Moshe, E. Farber, and G. Deutscher, *Phys. Rev. B* **99**, 224503 (2019).
- [10] A. Glezer Moshe, E. Farber, and G. Deutscher, *Appl. Phys. Lett.* **117**, 062601 (2020).
- [11] G. Deutscher, M. Gershenson, E. Grunbaum, and Y. Imry, *Journal of Vacuum Science and Technology* **10**, 697 (1973).
- [12] R. C. Dynes, J. P. Garno, G. B. Hertel, and T. P. Orlando, *Phys. Rev. Lett.* **53**, 2437 (1984).
- [13] F. Levy-Bertrand, T. Klein, T. Grenet, O. Dupré, A. Benoît, A. Bideaud, O. Bourrion, M. Calvo, A. Catalano, A. Gomez, J. Goupy, L. Grünhaupt, U. v. Luepke, N. Maleeva, F. Valenti, I. M. Pop, and A. Monfardini, *Phys. Rev. B* **99**, 094506 (2019).
- [14] G. Deutscher, H. Fenichel, M. Gershenson, E. Grunbaum, and Z. Ovadyahu, *Journal of Low Temperature Physics* **10**, 231 (1973).
- [15] S. Lerer, N. Bachar, G. Deutscher, and Y. Dagan, *Physical Review B* **90**, 214521 (2014).
- [16] R. C. Dynes, V. Narayanamurti, and J. P. Garno, *PRL* **41**, 1509 (1978).
- [17] D. C. Mattis and J. Bardeen, *PR* **111**, 412 (1958).
- [18] U. S. Pracht, N. Bachar, L. Benfatto, G. Deutscher, E. Farber, M. Dressel, and M. Scheffler, *Physical Review B* **93**, 100503 (2016).
- [19] J. Bardeen, L. N. Cooper, and J. R. Schrieffer, *Physical Review* **108**, 1175 (1957).
- [20] R. C. Dynes and J. P. Garno, *Phys. Rev. Lett.* **46**, 137 (1981).
- [21] L. Pisani, P. Pieri, and G. C. Strinati, *Phys. Rev. B* **98**, 104507 (2018).
- [22] L. Pisani, A. Perali, P. Pieri, and G. C. Strinati, *Phys. Rev. B* **97**, 014528 (2018).
- [23] P. W. Phillips, L. Yeo, and E. W. Huang, *Nature Physics* (2020).
- [24] A. Glezer Moshe, E. Farber, and G. Deutscher, *Phys. Rev. Research* **2**, 043354 (2020).
- [25] A. Spuntarelli, P. Pieri, and G. Strinati, *Physics Reports* **488**, 111 (2010).
- [26] B. Abeles, *Physical Review B* **15**, 2828 (1977).
- [27] N. Bachar, A. Levy, T. Prokscha, A. Suter, E. Morenzoni, Z. Salman, and G. Deutscher, *Phys. Rev. B* **101**, 024424 (2020).
- [28] R. Kubo, *Journal of the Physical Society of Japan* **17**, 975 (1962).
- [29] F. Yang, T. Gozlinski, T. Storbeck, L. Grünhaupt, I. M. Pop, and W. Wulfhekel, *PRB* **102**, 104502 (2020).
- [30] P. Winkel, K. Borisov, L. Grünhaupt, D. Rieger, M. Spiecker, F. Valenti, A. V. Ustinov, W. Wernsdorfer, and I. M. Pop, *PRX* **10**, 031032 (2020).
- [31] L. Grünhaupt, N. Maleeva, S. T. Skacel, M. Calvo, F. Levy-Bertrand, A. V. Ustinov, H. Rotzinger, A. Monfardini, G. Catelani, and I. M. Pop, *Phys. Rev. Lett.* **121**, 117001 (2018).
- [32] N. Maleeva, L. Grünhaupt, T. Klein, F. Levy-Bertrand, O. Dupre, M. Calvo, F. Valenti, P. Winkel, F. Friedrich, W. Wernsdorfer, A. V. Ustinov, H. Rotzinger, A. Monfardini, M. V. Fistul, and I. M. Pop, *Nature Communications* **9**, 3889 (2018).
- [33] F. Henriques, F. Valenti, T. Charpentier, M. Lagoin, C. Gouriou, M. Martínez, L. Cardani, M. Vignati, L. Grünhaupt, D. Gusenkova, J. Ferrero, S. T. Skacel, W. Wernsdorfer, A. V. Ustinov, G. Catelani, O. Sander, and I. M. Pop, *Appl. Phys. Lett.* **115**, 212601 (2020).
- [34] L. Grünhaupt, M. Spiecker, D. Gusenkova, N. Maleeva, S. T. Skacel, I. Takmakov, F. Valenti, P. Winkel, H. Rotzinger, W. Wernsdorfer, A. V. Ustinov, and I. M. Pop, *Nature Materials* **18**, 816 (2019).
- [35] F. Valenti, F. Henriques, G. Catelani, N. Maleeva, L. Grünhaupt, U. von Lüpke, S. T. Skacel, P. Winkel, A. Bilmes, A. V. Ustinov, J. Goupy, M. Calvo, A. Benoît, F. Levy-Bertrand, A. Monfardini, and I. M. Pop, *PRAPPLIED* **11**, 054087 (2019).
- [36] W. Zhang, K. Kalashnikov, W.-S. Lu, P. Kamenov, T. DiNapoli, and M. E. Gershenson, *PRAPPLIED* **11**, 011003 (2019).
- [37] P. Kamenov, W.-S. Lu, K. Kalashnikov, T. DiNapoli, M. T. Bell, and M. E. Gershenson, *PRAPPLIED* **13**, 054051 (2020).